J|A|C|S
ARTICLES
Published on Web 02/11/2006

Binding of Molecular O_2 to Di- and Triligated $[UO_2]^+$

Gary S. Groenewold,* Kevin C. Cossel, Garold L. Gresham, Anita K. Gianotto, Anthony D. Appelhans, John E. Olson, Michael J. Van Stipdonk,* and Winnie Chien

Contribution from the Department of Chemical Sciences, Idaho National Laboratory, 2525 North Fremont Avenue, Idaho Falls, Idaho 83415-2208, and Department of Chemistry, Wichita State University, Wichita, Kansas 67260

Received November 8, 2005; E-mail: gary.groenewold@inl.gov; mike.vanstipdonk@wichita.edu

Abstract: Gas-phase complexes containing dioxouranium(V) cations ($[UO_2]^+$) ligated with two or three σ-donating acetone ligands reacted with dioxygen to form $[UO_2(A)_{2,3}(O_2)]^+$, where A is acetone. Collision-induced dissociation studies of $[UO_2(A)_3(O_2)]^+$ showed initial loss of acetone, followed by elimination of O_2, which suggested that O_2 was bound more strongly than the third acetone ligand, but less strongly than the second. Similar behavior was observed for complexes in which water was substituted for acetone. Binding of dioxygen to $[UO_2]^+$ containing zero, one, or four ligands did not occur, nor did it occur for analogous ligated $U(IV)O_2$ or $U(VI)O_2$ ions. For example, only addition of acetone and/or H_2O occurred for the U(VI) species $[UO_2OH]^+$, with the ligand addition cascade terminating in formation of $[UO_2OH(A)_3]^+$. Similarly, the U(IV) species $[UOOH]^+$ added donor ligands, which produced the mixed-ligand complex $[UOOH(A)_3(H_2O)]^+$ as the preferred product at the longest reaction times accessible. Since dioxygen normally functions as an electron acceptor, an alternative mode for binding dioxygen to the cationic $U(V)O_2$ center is indicated that is dependent on the presence of an unpaired electron and donor ligands in the uranyl valence orbitals.

Introduction

The structure and reactivity of molecular uranium species have been topics of ongoing research because they dictate the behavior of the element at various junctures in the environment[1−3] and in the nuclear fuel cycle.[4,5] The envelope of possible species is broad and includes multiple oxidation states, oxide forms, ligand complexes, and multi-uranium clusters: each of these can display variable stability and solubilization depending on the composition, acidity, and oxidizing potential of a contacting solution.[6,7] Prediction and manipulation of uranium behavior are dependent on a detailed understanding of the reactivity of the salient species.

Positively charged, oxidized uranium species tend to act as Lewis acids, accepting electron density from donor ligands and participating in hydrolysis reactions at neutral pH. Uranium in the lower oxidation states is also highly oxophilic, as shown by several gas-phase studies that indicated oxidation by a number of neutral reagents. For example, gas-phase U^+ reacts with dioxygen to form UO^+, which reacts with a second O_2 to form the U(V) species UO_2^+.[8] In similar fashion, U^{2+} is oxidized to UO^{2+} and UO_2^{2+} in serial reactions with O_2 and other oxidants.[9,10] However, reactions of uranium cations with dioxygen to form complexes containing intact O_2 ligands have not been observed in the gas phase.

In the condensed phases, the uranyl dication forms complexes with dioxygen in an η^2-peroxo fashion,[11] including the uranyl peroxy minerals studtite $(UO_2)O_2(H_2O)_4$ and metastudtite $(UO_2)O_2(H_2O)_2$.[12] There are several examples in which two $[UO_2]^{2+}$ molecules are joined by peroxide in a μ-dioxo mode.[13−18] In these condensed-phase systems, a common theme is that binding of oxygen is very much dependent upon other ligands bound to the uranium center.

In contrast to peroxide binding, examples of superoxo dioxygen binding to actinide centers are scarce. Reversible attachment of dioxygen as superoxide to transition metal centers is well known,[19−24] and attachment of O_2^{2-} is central to the

(1) Morse, J. W.; Choppin, G. R. *Rev. Aquatic Sci.* **1991**, *4* (1), 1−22.
(2) Silva, R. J.; Nitsche, H. *Radiochim. Acta* **1995**, *70/71*, 377−396.
(3) Brookins, D. G. *Geochemical Aspects of Radioactive Waste Disposal*; Springer-Verlag: New York, 1984.
(4) Greenwood, N. N.; Earnshaw, A. *Chemistry of the Elements*, 2nd ed.; Butterworth Heinemann: Oxford, Great Britain, 1997; p 1250.
(5) Schulz, W. W.; Navratil, J. D. *Science and Technology of Tributyl Phosphate*; CRC Press: Boca Raton, FL, 1984.
(6) Choppin, G. R.; Rizkalla, E. N. Solution Chemistry of Actinides and Lanthanides. In *Handbook on the Physics and Chemistry of Rare Earths*; Gschneider, K. A., Jr., Eyring, L., Choppin, G. R., Lander, G. H., Eds.; Vol. 18, Lanthanides/Actinides: Chemistry; North-Holland: Amsterdam, 1994; pp 559−590.
(7) Rizkalla, E. N.; Choppin, G. R. Lanthanides and Actinides Hydration and Hydrolysis. In *Handbook on the Physics and Chemistry of Rare Earths*; Gschneider, K. A., Jr., Eyring, L., Choppin, G. R., Lander, G. H., Eds.; Vol. 18, Lanthanides/Actinides: Chemistry; North-Holland: Amsterdam, 1994; pp 529−558.
(8) Armentrout, P. B.; Beauchamp, J. L. *Chem. Phys.* **1980**, *50* (1), 27−36.
(9) Cornehl, H. H.; Heinemann, C.; Marcalo, J.; deMatos, A. P.; Schwarz, H. *Angew. Chem., Int. Ed. Engl.* **1996**, *35*, 891−894.
(10) Gibson, J. K.; Haire, R. G.; Santos, M.; Marcüalo, J.; Pires de Matos, A. *J. Phys. Chem. A* **2005**, *109*, 2768−2781.
(11) Alcock, N. W. *J. Chem. Soc. A* **1968**, 1588−1594.
(12) Kubatko, K.-A. H.; Helean, K. B.; Navrotsky, A.; Burns, P. C. *Science* **2003**, *302*, 1191−1193.
(13) Bhattacharjee, M.; Chaudhuri, M. K.; Purkayastha, R. N. D. *Inorg. Chem.* **1986**, *25*, 2354−2357.
(14) Charpin, P. P.; Folcher, G.; Lance, M.; Vigner, N. E. D. *Acta Crystallogr.* **1985**, *C41*, 1302−1305.
(15) Rose, D.; Chang, Y.-D.; Chen, Q.; Zubleta, J. *Inorg. Chem.* **1994**, *33*, 5167−5168.
(16) Thuery, P.; Masci, B. *Supramol. Chem.* **2003**, *15*, 95−99.
(17) Thuery, P.; Nierlich, M.; Baldwin, B. W.; Komatsuzaki, N.; Hirose, T. *J. Chem. Soc., Dalton Trans.* **1999**, 1047−1048.
(18) Westland, A. D.; Tarafder, M. T. H. *Inorg. Chem.* **1981**, *20*, 3992−3995.
(19) Momenteau, M.; Reed, C. A. *Chem. Rev.* **1994**, *94*, 659−698.

functioning of hemoglobin.[25] For actinide complexes, the autoxidation of $[UO_2]^+$ to form $[UO_2]^{2+}$ and peroxide[26] was speculated to proceed via a superoxo complex $[(UO_2)^{2+}(O_2)^-]$ in which uranium was formally oxidized to U(VI). With a single electron in its valence orbitals and an accessible higher metal oxidation state, $[UO_2]^+$ satisfies requirements for formation of a superoxo complex.[19] However, the chemistry of the U(V) dioxo cation is difficult to study in solution because of its tendency to undergo disproportionation[6,27−29] reactions in which two U(V) species react to form U(IV) and U(VI) species, with $[UO_2]^+$ functioning as both an electron donor and an electron acceptor.

The complexity of the uranium systems in the condensed phases obfuscates explicit identification of those factors that enable oxygen addition. On the other hand, the reactivity of ionic species can be examined more easily in the gas phase, because individual ionic species can be isolated prior to reaction. Recent studies have shown that reactions of gaseous uranium dioxo cations mirror their behavior in solution, in that noncovalent complexes form between donor ligands (e.g. H_2O,[30] alcohols,[31] or acetone[32]) and uranium(IV), -(V), and -(VI) dioxo cations. Unligated cations having 1+ and 2+ charges[30,32] and singly charged uranyl−anion ion pairs[33,34] behave in this fashion. Less frequently, uranium oxidation[30] or reduction[35] reactions occurred within the ligated complexes, but in the vast majority of cases, the cations acted as Lewis acids.

In the present report, we show that complexes containing the U(V) cation $[UO_2]^+$ will add molecular oxygen in the gas phase. In this study, the reactive motif of the U(V) species $[UO_2]^+$ is shown to be primarily that of a Lewis acid accepting electron density from donor ligands and forming noncovalent complexes in the process. However, it is shown that some ligand complexes of $[UO_2]^+$ will also add molecular dioxygen, suggesting donation of electron density from the metal center.

Experimental Section

The gas-phase reactivity experiments were conducted using two different types of quadrupole ion trap mass spectrometers, one using particle desorption for ionization (secondary ion mass spectrometry) and one using electrospray. The two instrumental approaches provided corroborating information.

Ion Trap Secondary Ion Mass Spectrometry (IT-SIMS). The ion trap secondary ion mass spectrometer (a Saturn 2000 ITMS from Varian (Walnut Creek, CA), modified using software written in-house)[36−38] is a unique instrument for examining the reactivity of metal oxide species. Briefly, it functions by bombarding solid metal oxide targets with a 7 keV ReO_4^- primary ion (obtained by applying a current of around 3 A to an amalgam of barium peroxide and rhenium powder),[39,40] which sputters ionic oxide species into the gas phase. In our experiments, the primary beam was gated to impact only the sample for the given ionization time. Ionization times were varied from 0.001 to 0.01 s to achieve high signal-to-noise ratios and comparable abundance (2000−4000 counts s^{-1}) for each of the reactant ions examined. The sputtered ions were trapped in a He bath gas (1×10^{-4} Torr), and the ion of interest was isolated using selected ion storage[41] prior to reaction with gaseous neutrals. The secondary ions used in this experiment were all generated by bombardment of uranium (VI) oxide (Strem Chemicals, Newburyport, MA).[30] The sample was mounted on the end of a 2.7-mm probe tip with double-sided tape (3M, St. Paul, MN). Isolated ions were then allowed to react with gaseous H_2O, acetone, and/or O_2 during a specified reaction time (0−3 s) that was systematically controlled. The ion trap was operated at a low mass cutoff of m/z 160 during the ionization and reaction time periods. After reaction, the product ions and remaining reactants were scanned out of the trap[41] and deflected onto a venetian blind dynode positioned in front of the multichannel plate detector, located off-axis between the end of the ion trap and the primary ion gun.[36]

To determine the reaction pathways and kinetics, the time between ion isolation and detection was systematically increased. Spectra were recorded at logarithmically increasing time intervals (approximately two measurements per decade) in order to concentrate data collection early in the ligand addition cascades, where the chemistry was rapidly changing. At long reaction times, spectra were not collected at closely spaced time intervals because the chemistry was not changing rapidly, and more importantly, the UO_3 target tended to develop surface charge under prolonged bombardment, which put a premium on data collection efficiency. At any given point in time, total ion abundance was normalized to 1000 ions, which was a convenient number for use in the kinetic modeling (vide infra).

As an alternative to condensation reactions, isolated complexes were subjected to collision-induced dissociation (CID).[41] Ions stabilized in the quadrupole ion trap have a coherent oscillating ion motion in the ion trap and a random component derived from the thermal energy of the system. Dissociation results from hyperthermal collisions with the bath gas that are induced by application of a potential on the end caps at a frequency corresponding to the secular frequency of the motion of the ion. Dissociation of metal complexes containing two or more different ligands produces fragment ions corresponding to the elimination of the ligands, whose relative intensities can be correlated with metal cation affinities.[42−44] Interpretation of the results of these studies is tempered by uncertainty regarding the effective temperature of the dissociating ions, the possibility of reverse activation energy, and the fact that ΔS may not be negligible;[45] however, in instances where the

(20) Dickman, M. H.; Pope, M. T. *Chem. Rev.* **1994**, *94*, 569−584.
(21) Karlin, K. D.; Tolman, W. B.; Kaderli, S.; Zuberbuhler, A. D. *J. Mol. Catal. A* **1997**, *117* (1−3), 215−222.
(22) Jones, R. D.; Summerville, D. A.; Basolo, F. *Chem. Rev.* **1979**, *79*, 139−179.
(23) Vaska, L. *Acc. Chem. Res.* **1976**, *9*, 175−183.
(24) Valentine, J. S. *Chem. Rev.* **1973**, *73*, 235−245.
(25) Pauling, L.; Coryell, C. D. *Proc. Natl. Acad. Sci. U.S.A.* **1936**, *22*, 210−216.
(26) Bakac, A.; Espenson, J. H. *Inorg. Chem.* **1995**, *34*, 1730−1735.
(27) Burgess, J. *Metal Ions in Solution*; Ellis Horwood Ltd.: Chichester, UK, 1978; p 481.
(28) Ekstrom, A. *Inorg. Chem.* **1974**, *13*, 2237−2241.
(29) Morris, D. E. *Inorg. Chem.* **2002**, *41*, 3542−3547.
(30) Gresham, G. L.; Gianotto, A. K.; Harrington, P. de B.; Cao, L.; Scott, J. R.; Olson, J. E.; Appelhans, A. D.; Van Stipdonk, M. J.; Groenewold, G. S. *J. Phys. Chem. A* **2003**, *107*, 8530−8538.
(31) Van Stipdonk, M. J.; Gresham, G.; Groenewold, G.; Anbalagan, V.; Hanna, D.; Chien, W. *J. Am. Soc. Mass Spectrom.* **2003**, *14*, 1205−1214.
(32) Van Stipdonk, M. J.; Chien, W.; Angalaban, V.; Bulleigh, K.; Hanna, D.; Groenewold, G. S. *J. Phys. Chem. A* **2004**, *108*, 10448−10457.
(33) Chien, W.; Hanna, D.; Anbalagan, V.; Gresham, G.; Groenewold, G.; Zandler, M.; Van Stipdonk, M. *J. Am. Soc. Mass Spectrom.* **2004**, *15*, 777−783.
(34) Anbalagan, V.; Chien, W.; Gresham, G. L.; Groenewold, G. S.; Van Stipdonk, M. J. *Rapid Commun. Mass Spectrom.* **2004**, *18*, 3028−3034.
(35) Van Stipdonk, M. J.; Chien, W.; Anbalagan, V.; Gresham, G. L.; Groenewold, G. S. *Int. J. Mass Spectrom.* **2004**, *237*, 175−183.
(36) Gresham, G. L.; Groenewold, G. S.; Olson, J. E. *J. Mass Spectrom.* **2000**, *35*, 1460−1469.
(37) Groenewold, G. S.; Appelhans, A. D.; Ingram, J. C. *J. Am. Soc. Mass Spectrom.* **1998**, *9*, 35−41.
(38) Groenewold, G. S.; Appelhans, A. D.; Ingram, J. C.; Gresham, G. L.; Gianotto, A. K. *Talanta* **1998**, *47*, 981−986.
(39) Delmore, J. E.; Appelhans, A. D.; Peterson, E. S. *Int. J. Mass Spectrom. Ion Processes* **1995**, *146/147*, 15−20.
(40) Johnson, K. B.; Delmore, J. E.; Appelhans, A. D. *Int. J. Mass Spectrom.* **2003**, *229*, 157−166.
(41) Todd, J. F. J. *Practical Aspects of Ion Trap Mass Spectrometry*; CRC Press: New York, 1995; Vol. 1, p 4.
(42) Brodbelt-Lustig, J. S.; Cooks, R. G. *Talanta* **1989**, *36* (1/2), 255−260.
(43) Cooks, R. G.; Patrick, J. S.; Kotaiho, T.; McLuckey, S. A. *Mass Spectrom. Rev.* **1994**, *13*, 287−339.
(44) Nourse, B. D.; Cooks, R. G. *Int. J. Mass Spectrom. Ion Processes* **1991**, *106*, 249−272.
(45) Armentrout, P. B. *J. Mass Spectrom.* **1999**, *34*, 74−78.

mechanism for elimination of two ligands is similar,[46] the fragmentation kinetics as reflected by the relative abundances of the fragment ions can be suggestive of the relative binding energies of the eliminated ligands.

The atmosphere within the ion trap secondary ion mass spectrometer was modified by the addition of low partial pressures of acetone, H_2O, and O_2 to the He bath gas. Acetone (Optima grade, Fisher, Fairlawn, NJ) was first dried with molecular sieves, which were previously heated to ~175 °C and allowed to cool, to remove any dissolved water. The acetone was then subjected to several freeze−pump−thaw cycles with liquid nitrogen while connected to a roughing vacuum pump. The acetone was then admitted to the system as a vapor through a variable-leak valve. Oxygen (UHP, Matheson, Newark, CA) and $^{18}O_2$ (99% enrichment, Isotec-Matheson, Miamisburg, OH) were admitted using a separate variable-leak valve. A third variable-leak valve was used to admit water (Optima grade, Fisher, Fairlawn, NJ), which was also subjected to three freeze−pump−thaw cycles with liquid nitrogen while under vacuum.

Calculation of reaction rate constants is critically dependent on accurate determination of the number density of the reactant neutrals. Pressure measurement was accomplished using a small electron ionization quadrupole mass spectrometer (Transpector 2 residual gas analyzer, Inficon, East Syracuse, NY) that was interfaced to the ion trap secondary ion mass spectrometer and was operated to continuously monitor ion channels corresponding to the components of the vacuum atmosphere, viz., He, H_2O, N_2, O_2, and acetone. The quadrupole mass spectrometer was carefully calibrated versus a Bayard Alpert ionization gauge. The ionization gauge was, in turn, calibrated against a capacitance manometer for each gas except He, which was maintained at a pressure of 1×10^{-4} Torr as measured by the quadrupole mass spectrometer and checked with the ionization gauge.

Electrospray Ionization Mass Spectrometry (ESI-MS). ESI mass spectra were collected using a Finnigan LCQ-Deca ion trap mass spectrometer (ThermoFinnigan Corp., San Jose, CA). The spray solutions used in these experiments consisted of the uranyl nitrate dissolved to a concentration of 1 mM in 10% (v:v) acetone/water. The solutions were infused into the ESI-MS instrument using the incorporated syringe pump at a flow rate of 3−5 μL/min.

The atmospheric pressure ionization stack settings for the LCQ instrument (lens voltages, quadrupole, octapole voltage offsets, etc.) were optimized for maximum ion transmission to the ion trap mass analyzer by using the autotune routine within the LCQ Tune program. Following the instrument tune, the spray needle voltage was maintained at +5 kV and the N_2 sheath gas flow at 25 units (arbitrary to the LCQ instrument, corresponding to approximately 0.375 L/min). The heated capillary (desolvation) temperature was maintained 250 °C. At this relatively high desolvation temperature, the ESI mass spectrum was dominated by singly charged species including bare and ligated UO_2-OH^+, $UO_2NO_3^+$, and UO_2^+. The ion trap analyzer was operated at a pressure of $\sim 1.5 \times 10^{-5}$ Torr. Helium gas, admitted directly into the ion trap, was used as the bath/buffer gas to improve trapping efficiency and as the collision gas for CID experiments. To investigate the tendency to add molecular O_2 via gas-phase reactions, a certified blend of He with 0.1 or 1.0% O_2 (Linweld, Wichita, KS) was used.

Ligand addition reactions (H_2O and/or O_2) were monitored by the isolation and storage of the UO_2^+ ion in the ion trap. The O_2 reagent was introduced with the He bath gas. The H_2O is a contaminant in the vacuum system and has been shown in past studies to be present at partial pressures sufficient to produce pseudo-first-order reaction conditions. In the present experiments, H_2O added to UO_2^+ in the electrospray ion trap. At the acetone concentration used in the spray solvent mixture, no appreciable acetone addition to UO_2^+ complexes was observed. The multiple-stage CID experiments[31] were performed by setting the isolation width between 5 and 12 mass units (depending on the species), the activation Q at 0.3 (as labeled by the instrument manufacturer, used to adjust the q_z value for the resonant excitation of the precursor ion during the CID portion of the experiment), and the activation amplitude at 10−20% (of 5 V). In all cases, activation times for CID were 30 ms.

Kinetic Modeling. Kinetic rates were extracted from the data by using the curve fit feature of Berkeley Madonna,[47] which is a commercially available, general purpose differential equation solver that utilizes a numerical Runge−Kutta integration algorithm. This program uses the downhill simplex method as documented in *Numerical Methods in C* for curve fitting.[48] The model used for this fit was based on a pseudo-first-order approximation of the reactions with respect to the acetone, oxygen, and water concentrations. Rate constants were obtained by dividing the rates from Berkeley Madonna by the number density of the secondary reactant (e.g., acetone). The ability of the model to fit the data was assessed for each ion modeled by calculating the root-mean-square error (RMS) between the data and the model for each time at which a data point was collected and expressing the value as a percentage of the average ion abundance over the time course of the experiment. Good fits were indicated by %RMS values from 1% to ~30%, which was the case for the abundant ions in the forward ligand attachment cascades. Lower abundance ions could have values several times higher, but they still produced fits for models of simple ligand addition and elimination that were good qualitative fits of the data points.

Infrared Multiphoton Dissociation (IRMPD). An IRMPD experiment on the $[UO_2(\text{dimethylformamide})_{n=2,3}(O_2)]^+$ complex was conducted using a free electron laser interfaced to a Fourier transform ion cyclotron resonance mass spectrometer at the FOM Instituut voor Plasmafysica, Nieuwegein, The Netherlands. The experiment was described previously.[49,50] Complexes were formed using electrospray as described above, except using dimethylformamide instead of acetone. Complexes were isolated using the stored waveform inverse Fourier transform technique[51] and then dissociated by photoirradiation of the isolated complex ions.

Results and Discussion

Reactions of the U(V) Species $[UO_2]^+$. The U(V) species $[UO_2]^+$ accounted for the most abundant ion in the SIMS spectrum of UO_3 at m/z 270. The major ions that emerged upon reaction of $[UO_2]^+$ in an atmosphere containing acetone (A), H_2O, and O_2 were as follows. After 0.06 s, a substantial fraction of $[UO_2]^+$ was converted to $[UO_2(A)]^+$ (Figure 1a), and some of this had further reacted to form diligated $[UO_2(A)(H_2O)]^+$ and $[UO_2(A)_2]^+$ (Schemes 1 and 1S (Supporting Information)). After 0.3 s, abundant triligated complexes having compositions $[UO_2(A)_2(H_2O)]^+$ and $[UO_2(A)_3]^+$ formed, and some of these were converted to the tetraligated $[UO_2(A)_4]^+$ (Figure 1b). The $[UO_2(A)_4]^+$ represented the end of the ligand addition cascade, involving only acetone and H_2O. In contrast to the behavior of ligated $[UO_2]^{2+}$ in the gas phase,[32] pentaligated $[UO_2]^+$ complexes were not formed at the longest times experimentally accessible.

Most important to the present study, an ion was observed at m/z 476. This species corresponds to the addition of O_2 to the

(46) Green-Church, K. B.; Limbach, P. A. *J. Am. Soc. Mass Spectrom.* **2000**, *11*, 24−32.
(47) Zahnley, T.; Macey, R.; Oster, G. *Berkeley Madonna*, version 8.0.1; University of California: Berkeley, CA, 2003.
(48) Flowers, B. H. *Numerical Methods in C*$^{++}$, 2nd ed.; Oxford University Press: New York, 2000.
(49) Moore, D. T.; Oomens, J.; Eyler, J. R.; Meijer, G.; von Helden, G.; Ridge, D. P. *J. Am. Chem. Soc.* **2004**, *126*, 14726−14727.
(50) Oomens, J.; Moore, D. T.; von Helden, G.; Meijer, G.; Dunbar, R. C. *J. Am. Chem. Soc.* **2004**, *126*, 724−725.
(51) Marshall, A. G.; Wang, J. T.-C. L.; Ricca, T. L. *J. Am. Chem. Soc.* **1985**, *107*, 7893−7897.

Scheme 1. Main Reaction Pathways for the Addition of Acetone, H_2O, and/or O_2 to $[UO_2]^+$, Occurring in the Ion Trap Secondary Ion Mass Spectrometer[a]

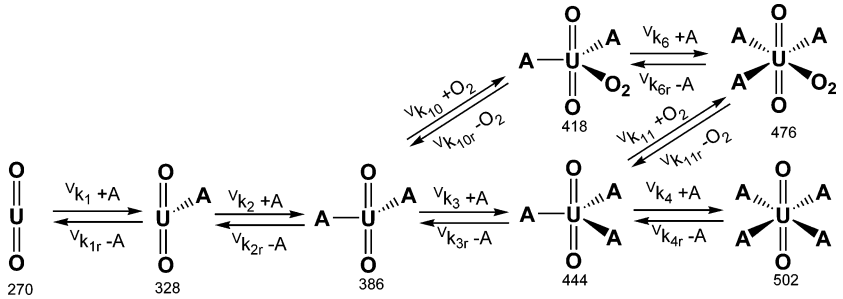

[a] The complete reaction scheme, which includes lower abundance ions, is found in the Supporting Information, Scheme 1S.

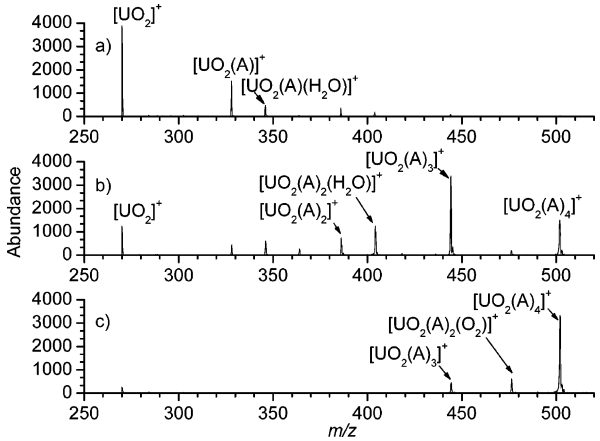

Figure 1. $[UO_2]^+$ formed and isolated in the vacuum atmosphere of the ion trap secondary ion mass spectrometer. Water and dioxygen were present at background concentrations ($\sim 5 \times 10^{-7}$ Torr), and acetone was added to a pressure of $\sim 1 \times 10^{-6}$ Torr. The $[UO_2]^+$ reacted for (a) 0.06, (b) 0.3, and (c) 3 s.

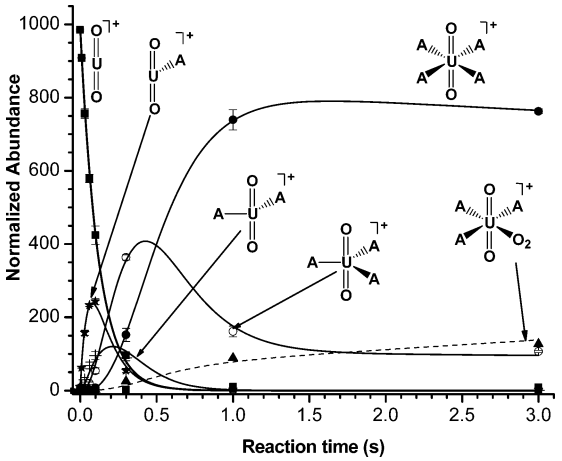

Figure 2. Kinetic profile for the major reactions formed from $[UO_2]^+$ in an atmosphere containing acetone, H_2O, and dioxygen. Data points represent the average of three runs. Lines represent the plot of the kinetic model for each of the ions.

$[UO_2(A)_3]^+$ complex. At the longest times of these experiments, all of the ion abundance was contained in $[UO_2(A)_4]^+$ and $[UO_2(A)_3(O_2)]^+$ (Figure 1c).

The temporal variations of the ions observed in this experiment enabled the reaction pathway in Schemes 1 and 1S to be deduced, and thus allowed the development of a kinetic model that produced reaction profiles in good agreement with the measured data (Figure 2). The model was developed using ligand association and dissociation reactions that were assumed to be bimolecular and unimolecular, respectively. This is a simplified description of the actual physical system, in which the reactions are ternary[52,53] in the reactant ion, the neutral ligand, and the He bath gas; the latter reduces internal energy in the initially formed complexes, and hence the rate of dissociation reactions. Ligand exchange reactions between complexes were not considered because of low ion concentrations in the instrument.

Table 1. Forward Rate Constant Values for Addition of Acetone to $[UO_2]^+$ [a]

forward reaction	rate const., $^{V}k_n$	mean $^{V}k_n$ values	% efficiency (relative to k_{ADO})
$[UO_2]^+ + A \rightarrow [UO_2(A)]^+$	$^{V}k_1$	2×10^{-10}	10
$[UO_2(A)]^+ + A \rightarrow [UO_2(A)_2]^+$	$^{V}k_2$	2×10^{-10}	10
$[UO_2(A)_3]^+ + A \rightarrow [UO_2(A)_3]^+$	$^{V}k_3$	5×10^{-10}	20
$[UO_2(A)_3]^+ + A \rightarrow [UO_2(A)_4]^+$	$^{V}k_4$	9×10^{-11}	4
$[UO_2(A)_2]^+ + O_2 \rightarrow [UO_2(A)_2(O_2)]^+$	$^{V}k_{10}$	2×10^{-11}	3
$[UO_2(A)_3]^+ + O_2 \rightarrow [UO_2(A)_3(O_2)]^+$	$^{V}k_{11}$	1×10^{-11}	3

[a] The rate constant (k) values are in $cm^3\ s^{-1}$ molecule^{-1}. Table S1 in the Supporting Information contains rates calculated for all modeled addition reactions, and Table S2 contains rates for elimination reactions.

In this experiment, the dominant reaction pathway was addition of acetone, reflected by the substantial reaction efficiencies (compared with average dipole orientation theory[54−57]) of reactions 1−3 (Tables 1 and S1). The efficiency for the addition of the fourth acetone was somewhat lower, which may be the effect of ligands shielding the reactive center for many approach trajectories. In addition, steric crowding of the $[UO_2(A)_4]^+$ appears to lead to greater complex instability, as reflected in the modeled rate constants for acetone elimination (Table S2). The tetraligated complex had the largest rate constant for acetone elimination, and the observed trend was $[UO_2(A)_4]^+ > [UO_2(A)]^+ > [UO_2(A)_3]^+ > [UO_2(A)_2]^+$. Even with the elimination reactions, the overall addition of acetone in the gas phase was efficient, an observation that is consistent with the fact that the ligand is a strong σ-donor in the gas phase.[58,59] The efficiency observed contrasts with solution-phase behavior, in which acetone is a weakly binding ligand.[27,60,61] The

(52) Gilbert, R. G.; Smith, S. C. *Theory of Unimolecular and Recombination Reactions*, 1st ed.; Blackwell Scientific Publications: London, 1990.
(53) Weishaar, J. C. *Acc. Chem. Res.* **1993**, *26*, 213−219.
(54) Su, T.; Bowers, M. T. *J. Am. Chem. Soc.* **1973**, *95*, 7609−7610.
(55) Su, T.; Bowers, M. T. *J. Am. Chem. Soc.* **1973**, *95*, 7611−7613.
(56) Su, T.; Bowers, M. T. *Int. J. Mass Spectrom. Ion Phys.* **1973**, *12*, 347−356.
(57) Su, T.; Chesnavich, W. J. *J. Chem. Phys.* **1982**, *76*, 5183−5185.
(58) Eller, K.; Schwarz, H. *Chem. Rev.* **1991**, *91*, 1121−1177.
(59) Rodgers, M. T.; Armentrout, P. B. *Mass Spectrom. Rev.* **2000**, *19*, 215−247.
(60) Bardin, N.; Rubini, P.; Madic, C. *Radiochim. Acta* **1998**, *83*, 189−194.

preference of $[UO_2]^+$ cations for acetone observed in the present study was also consistent with a recent investigation of gas-phase $[UO_2]^{2+}$ complexes[32] and with the high coordination energy of uranyl acetone complexes recently calculated by Marsden and co-workers.[62]

Side reactions with gaseous H_2O were also observed. The efficiency of H_2O addition was higher for the monoacetone ligated $[UO_2]^+$ species (reactions 7 and 9 in Scheme 1S) than for the diacetone complex (reaction 8). The temporal behavior of the lower abundance H_2O-containing complexes is provided in Figure S1. For unligated $[UO_2]^+$, $[UO_2(A)_3]^+$, or $[UO_2(A)_4]^+$, addition of water did not occur to a measurable extent. The fact that H_2O did not add to $[UO_2]^+$ was somewhat surprising because this reaction occurs in the absence of acetone,[30] although relatively inefficient (ca. 3%) and with a fast back reaction. Addition of H_2O to the $[UO_2]^+$ di-, tri-, and tetraligated with acetone can be viewed similarly (i.e., occurring with poor efficiency and/or fast reverse reactions). On the other hand, addition of H_2O to $[UO_2(A)]^+$ was remarkably efficient, which is reflected in the notable abundance of $[UO_2(A)(H_2O)]^+$ in Figure 1a. The $[UO_2(A)(H_2O)]^+$ species was not quickly stabilized, having a relatively large rate constant for elimination of H_2O. Also observed were the addition of a second H_2O or acetone ligand to form $[UO_2(A)(H_2O)_2]^+$ and $[UO_2(A)_2(H_2O)]^+$ at intermediate times. The fact that $[UO_2(A)(H_2O)]^+$ was formed in abundance likely reflects a fortuitous combination of a highly undercoordinated uranium cation with sufficient oscillators in the first acetone ligand enabling stabilization of the complex. Addition of H_2O to complexes containing more than one acetone may not occur because additional electron density contributed by the multiple acetone ligands lessens the ability of the weaker H_2O ligand to form stable bonds with uranium.

At the longest reaction times, no H_2O-containing complexes remained; the rate constant for elimination of H_2O from $[UO_2(A)_2(H_2O)]^+$ was about 50 times greater than that for the elimination of acetone (Table S2), which is another indication of the much stronger binding of acetone in these systems. The net result of the more weakly bound H_2O-containing complexes with continued substitution by more strongly binding acetone is that eventually no H_2O complexes survive in the ion trap.

The most interesting observation, however, was the tendency of di- and triligated $[UO_2]^+$ to add O_2 (Scheme 1, reactions 10 and 11). The addition was plainly observed at *m*/*z* 476, corresponding to $[UO_2(A)_3(O_2)]^+$ (Figure 1c), and showed up at longer reaction times when most of the ion population had been converted to either tri- or tetraligated species. The $[UO_2(A)_3(O_2)]^+$ showed no tendency to add an additional ligand, suggesting that the coordination sites were fully occupied and that the precursor was $[UO_2(A)_3]^+$. The identification of the dioxygen adduct was confirmed in two ways: first, addition of O_2 to the ion trap secondary ion mass spectrometer resulted in production of a higher fraction of $[UO_2(A)_3(O_2)]^+$ compared with the other terminal product $[UO_2(A)_4]^+$, and second, addition of $^{18}O_2$ to the ion trap shifted the mass of the product to *m*/*z* 480, consistent with the proposed composition.

Subsequent experiments that utilized the electrospray ion trap (vide infra) indicated that diligated $[UO_2]^+$ also reacted with

Scheme 2. Reaction Pathways for the Addition of H_2O and/or O_2 to $[UO_2A]^+$, Occurring in the ESI Ion Trap

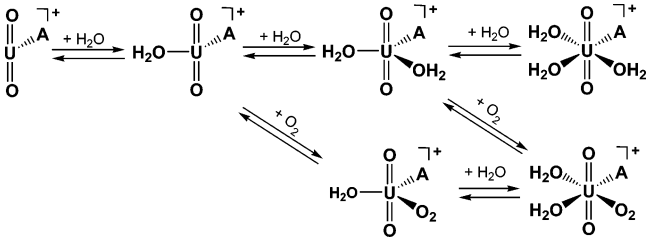

Scheme 3. Serial Collision-Induced Dissociation Reactions of the U(V) Species $[UO_2(A)_3(O_2)]^+$, Suggesting Alternating Ligand Binding Depending on the Extent of Ligation

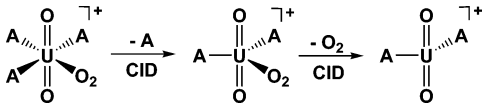

O_2 to form stable complexes, and this prompted a more thorough examination of the IT-SIMS results. A low-abundance ion formed at *m*/*z* 418 corresponded to $[UO_2(A)_2(O_2)]^+$ formed from $[UO_2(A)_2]^+$. Thus, both diacetone and triacetone $[UO_2]^+$ complexes reacted with O_2 to form stable adducts. In contrast, there was nothing in the mass spectra at any time frame to indicate addition of O_2 to tetra-, mono-, or unligated $[UO_2]^+$.

These conclusions were substantiated by the reactions observed in the ESI ion trap experiments. The $[UO_2(A)]^+$ species was generated as a stable species by ESI using the relatively high capillary/desolvation temperature of 250 °C. With the conditions employed in the ESI experiments, the predominant neutral reagents present in the ion trap were adventitious H_2O and O_2 that were admitted with the He bath gas. In this environment, $[UO_2(A)]^+$ added one H_2O to form $[UO_2(A)(H_2O)]^+$ (Scheme 2), but $[UO_2(A)]^+$ did not add O_2.

The diligated adduct then added O_2 to generate $[UO_2(A)(H_2O)(O_2)]^+$, and it also added a second H_2O to form $[UO_2(A)(H_2O)_2]^+$. At longer reaction times, $[UO_2(A)(H_2O)_2(O_2)]^+$ was also formed: an analysis of the kinetic evolution of the ion abundances showed that this ion was formed both from addition of O_2 to $[UO_2(A)(H_2O)_2]^+$ and from addition of H_2O to $[UO_2(A)(H_2O)(O_2)]^+$. The tetraligated $[UO_2(A)(H_2O)_3]^+$ was also formed in this experiment but showed no tendency to further react by adding O_2.

Ligand binding was assessed by fragmenting the dioxygen complexes:[42−44] $[UO_2(A)_3(O_2)]^+$ was subjected to CID by applying an axial excitation frequency to the ions, which increased the average kinetic energy of the collisions of the complexes with the He bath gas.[41] This resulted in preferential elimination of acetone (Scheme 3), and subsequent CID of the $[UO_2(A)_2(O_2)]^+$ produced the opposite result, viz., O_2 was lost instead of acetone (i.e., no $[UO_2(A)(O_2)]^+$ was detected, indicating that it was at least 200 times less intense than the ion from O_2 loss). These results suggest that the binding energy of O_2 is intermediate between those of the second and third acetone ligands.

Conclusions on relative binding energy based on competitive fragmentation reactions must be considered with caution, because of uncertainty arising from the possibility of reverse activation energy, unequal reaction entropy changes, and variation in dissociation rates with variable kinetic energy. In the present case, reverse activation energies are negligible, but

(61) Fratiello, A.; Kubo, V.; Lee, R. E.; Schuster, R. E. *J. Phys. Chem.* **1970**, *74*, 3726−3730.
(62) Clavaguera-Sarrio, C.; Hoyau, S.; Ismail, N.; Marsden, C. J. *J. Phys. Chem. A* **2003**, *107*, 4515−4525.

Scheme 4. Serial Addition of H_2O to the U(VI) Species $[UO_2((A-H)]^+$, Occurring in the ESI Ion Trap, Where (A−H) Is Deprotonated Acetone

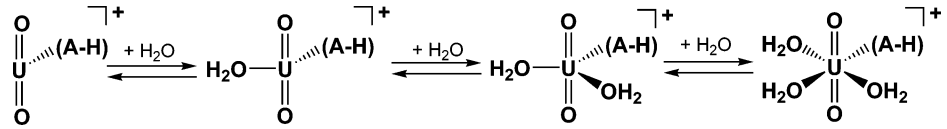

variable entropy changes on elimination of acetone versus O_2 may alter conclusions on relative ligand binding strength in the $[UO_2(A)_2(O_2)]^+$ complex. If the entropy change for elimination of acetone is equivalent to that for elimination of O_2, then the fact that only O_2 elimination is observed would indicate that it is less tightly bound than acetone. However, the entropy increase on loss of acetone could conceivably be smaller, because C−O rotation may decrease upon elimination: if the C−O bond in the complex is predominantly a single bond, re-formation of the carbonyl double bond upon elimination would reduce rotation and cause a smaller increase in entropy for the overall process. A smaller entropy change for loss of acetone would add to the energetic requirements for elimination of acetone compared to loss of O_2, and in the extreme case, this could result in loss of O_2, even though the bond energy of acetone is less than that of O_2. However, recent infrared experiments have shown that the double-bond character of the acetone carbonyl is not seriously compromised in triligated uranyl complexes (vide infra);[63] thus, it is unlikely that entropic considerations will change the order of ligand binding suggested by the CID experiments in this system. The conclusion is further substantiated by analogous CID behavior observed in the ESI ion trap for $[UO_2(A)(H_2O)_2(O_2)]^+$, which eliminated H_2O in the first fragmentation stage and then O_2 in the second; in this system, elimination of H_2O would lead to a lower net entropy change than would elimination of acetone.

Variable fragmentation with respect to kinetic energy is a second source of uncertainty. However, changes in the ratio of product ion abundances arising from competitive simple ligand cleavages were not observed over the energies available in the quadrupole ion trap. The order of ligand elimination was further evaluated by infrared multiphoton dissociation[49,50] of $[UO_2(ligand)_3(O_2)]^+$, where the ligand was the carbonyl species dimethylformamide. In the IRMPD experiment, the dominant reaction observed for $[UO_2(amide)_3(O_2)]^+$ was loss of a single amide. While loss of (amide + O_2) was also observed as a minor pathway, *no* loss of only O_2 was observed.[63] In contrast, the IRMPD behavior of $[UO_2(amide)_2(O_2)]^+$ showed elimination of only O_2, which indicated that, in the more undercoordinated complex, the O_2 ligand was less strongly bound than the amide ligands. The IRMPD experiments were consistent with the CID studies of the UO_2^+ complexes containing acetone or H_2O and bound molecular O_2, suggesting that the strength of O_2 binding is intermediate between those of the second and third carbonyl ligands.

Taken together, the condensation and fragmentation experiments show that the ligand field plays a controlling role in dictating whether O_2 binding will occur, as does the presence of an unpaired electron in the valence orbital of the metal. The importance of the U(V) oxidation state in O_2 binding was highlighted by the reactivity of U(VI) and U(IV) dioxo cations, which did not bind dioxygen in a molecular fashion.

(63) Groenewold, G. S.; Van Stipdonk, M. J.; Oomens, J.; Polfer, N.; Gianotto, A. K., unpublished results.

Reactions of the U(VI) Species $[UO_2OH]^+$ and $[UO_2(A-H)]^+$. Complexes containing uranium in the VI oxidation state nominally have no electrons in the valence orbitals to react with dioxygen, and they hence were not expected to form stable O_2-containing complexes. Nevertheless, the experience with the U(V) system indicated the possibility of ligands altering the reactivity of the metal center, which prompted investigation of reactions of uranyl complexes in oxygen-containing atmospheres. Addition of O_2 to uranyl systems was not observed to occur, and this was most vividly illustrated by examining the reactions of the U(VI) complex $[UO_2(A-H)]^+$ (where (A−H) is deprotonated acetone), which was formed in the ESI ion trap experiment by CID.

Analysis of a uranyl/acetone/water solution showed a tetraligated complex $[UO_2(A-H)(A)_3]^+$ at *m*/*z* 501 that was converted to $[UO_2(A-H)]^+$ by consecutive CID eliminations of three acetone ligands. The trapped product ion then reacted with three water ligands in serial fashion, forming $[UO_2(A-H)(H_2O)_{n=1-3}]^+$ (Scheme 4). This result, and those for the hydroxy uranyl species, underscores the importance of the unpaired electron in the U(V) species for fostering O_2 addition: in the present even-electron case, the ligand in $[UO_2(A-H)]^+$ is isoelectronic with the ligand in the U(V) species $[UO_2(A)]^+$ described above, the only difference being the presence of a proton in the latter. The consequence of the "missing" proton in the U(VI) complex is large, however, since it results in a negative charge on the ligand with no electron localized in the uranium valence orbitals: this eliminates the possibility of forming a stable complex with dioxygen.

The reactions of the analogous hydroxy uranyl cation reinforced this conclusion.[33] The production of $[UO_2OH]^+$ at *m*/*z* 287 (Figure 3a) in the ion trap secondary ion mass spectrometer afforded the opportunity to examine the behavior of a second U(VI) species reacting competitively with acetone, water, and dioxygen. The principal conclusion from the experiment was that the hydroxyuranyl cation failed to add O_2 at any point, regardless of the nature or extent of ligation. At all reaction times, the chemistry was dominated by addition of acetone ligands, which occurred for $[UO_2OH]^+$ to the exclusion of H_2O; this was surprising since water was shown to add, albeit at a slow rate, in a previous study.[30] At intermediate reaction times, $[UO_2OH]^+$ complexes containing two acetone ligands were formed (Figure 3b), and at the longest times, $[UO_2OH(A)_3]^+$ was produced (Figure 3c). The temporal profiles of the abundances of these ions (Figure 4) indicated the reaction pathway described in Scheme 5, reactions 1−3.

Reaction efficiencies for the acetone additions to the hydroxide complexes were 10−20% (Tables 2 and S4). Addition of a fourth acetone, generating an ion with five equatorial ligands, was not observed at any point. The rate constants calculated for elimination of acetone ligands from the complexes (Table S5) reveal a trend $[UO_2OH(A)_3]^+ \sim [UO_2OH(A)]^+ > [UO_2OH(A)_2]^+$. With more than four equatorial ligands, the rate for

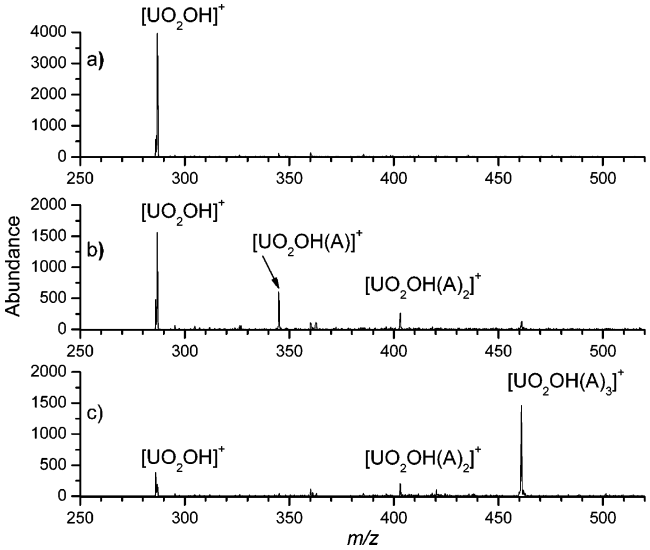

Figure 3. $[UO_2OH]^+$ formed and isolated in the vacuum atmosphere of the ion trap secondary ion mass spectrometer. Water and dioxygen were present at background concentrations ($\sim 5 \times 10^{-7}$ Torr), and acetone was added to a pressure of $\sim 1 \times 10^{-6}$ Torr. $[UO_2]^+$ reacted for 0.01 (top), 0.3 (center), and 1 s (bottom).

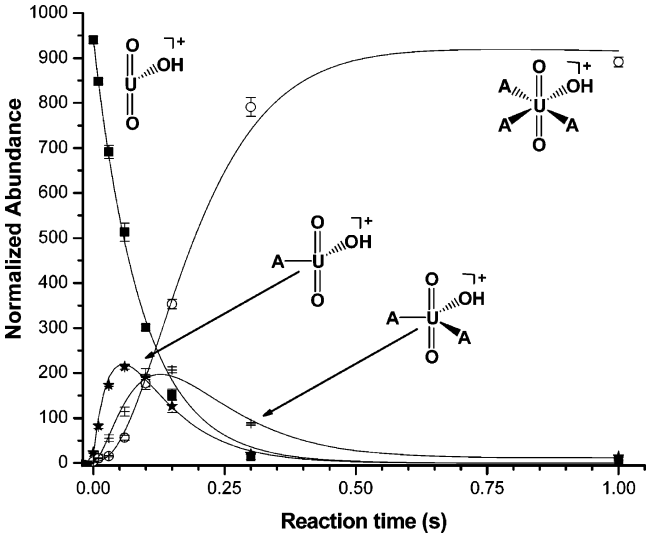

Figure 4. Kinetic profiles of the major ions formed from $[UO_2OH]^+$ in an atmosphere containing acetone, H_2O, and dioxygen. Abundances normalized to 1000 ions total (see Scheme 3) are plotted versus time. Data points represent the average of three runs; error bars represent ± 1 standard deviation. Lines represent the plot of the kinetic model for each of the ions, generated using the mean data values. See Figure S2 (Supporting Information) for the kinetic profiles of the lower abundance ions.

Scheme 5. Reaction Pathways for the Addition of Acetone and/or H_2O to $[UO_2OH]^+$, Occurring in the Ion Trap Secondary Ion Mass Spectrometer[a]

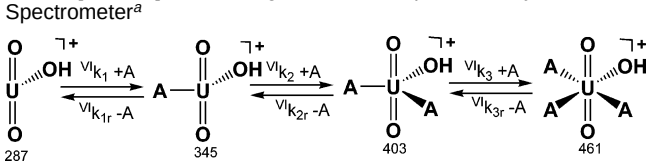

[a] The full scheme is found in the Supporting Information, Scheme 5S.

acetone elimination is presumably even faster, as the hydroxy complex with five equatorial ligands is not observed at all.

During the course of the acetone addition reactions, side reactions (Scheme 5S) produced low-abundance ions from the addition of H_2O to $[UO_2OH(A)]^+$ and $[UO_2OH(A)_2]^+$, but at no point did the abundance of these ions reach more than a few percent of the total ion population, and at the longest reaction times, they were not observed. The kinetic profile modeled for the low-abundance ions (Figure S2) produced good agreement with the data for all ions, except for low-abundance ion $[UO_2OH(A)(H_2O)]^+$, which formed and disappeared at a rate that was faster than could be reasonably modeled: the addition of H_2O to $[UO_2OH(A)]^+$ was modeled at a rate faster than the maximum indicated by the collision constant, which suggested that there may be additional reactions forming $[UO_2OH(A)(H_2O)]^+$. At the longest reaction times, no H_2O-containing complexes were present in the spectra, suggesting that (as for the U(V) complexes described above) the water-containing complexes slowly eliminate H_2O, forming species that continued to react with acetone. This implies that the H_2O-containing complexes are less stable than those containing only acetone, and the rate constants produced by the kinetic model were 2 orders of magnitude higher for elimination of H_2O than for elimination of acetone for complexes having the same extent of ligation (elimination rate constants are provided in the Supporting Information, Table S5).

Table 2. Forward Rate Constant Values for Addition of Acetone to $[UO_2OH]^+$ [a]

forward reaction	rate const., $^{VI}k_n$	mean $^{VI}k_n$ values	% efficiency (relative to k_{ADO})
$[UO_2OH]^+ + A \rightarrow [UO_2OH(A)]^+$	$^{VI}k_1$	3×10^{-10}	10
$[UO_2OH(A)]^+ + A \rightarrow [UO_2OH(A)_2]^+$	$^{VI}k_2$	5×10^{-10}	20
$[UO_2OH(A)_2]^+ + A \rightarrow [UO_2OH(A)_3]^+$	$^{VI}k_3$	5×10^{-10}	20

[a] The rate constant (k) values are in $cm^3\ s^{-1}\ molecule^{-1}$. Table S4 in the Supporting Information contains rates calculated for all modeled addition reactions, and Table S5 contains rates for elimination reactions.

A second set of low-abundance ions were observed at m/z 327, 385, 443, and 501 (Scheme 5S), corresponding to $[UO_2(A-H)(A)_{n=0-3}]^+$. The (A−H) represents deprotonated acetone (the enolate), and a reasonable suggestion for its initial formation would be H transfer from an acetone to the hydroxy ligand, forming a complex containing (A−H) and water. This complex was observed in ESI-MS experiments (see above) and can eliminate H_2O. The resulting enolate ion then undergoes addition of up to three additional acetone molecules. Rate constants for sequential addition of the acetone ligands to the enolate complexes were somewhat imprecise (Table S4), which reflected uncertainty in measurement of the low abundances of the enolate-bearing ions rather than reactivity trends; this limitation notwithstanding, the reaction pathway involving addition of acetone ligands to the $[UO_2(A-H)]^+$ complex is reasonable and accounts for the appearance of these ions at various times during the course of the ligand addition cascade.

These cascading ligand addition reactions showed that the uranyl−anion pair complexes were highly reactive, functioning as Lewis acids toward electron-donating ligands, but at no point was molecular addition of dioxygen observed, which was similar to the behavior of complexes of yet another dioxo uranium ion, $[UOOH]^+$.

Reactions of the U(IV) Species $[UOOH]^+$. The reactions of $[UOOH]^+$ were studied by IT-SIMS, where the ion was made in sufficient abundance to enable reactivity investigations, but were not studied by ESI-MS because there was not a facile

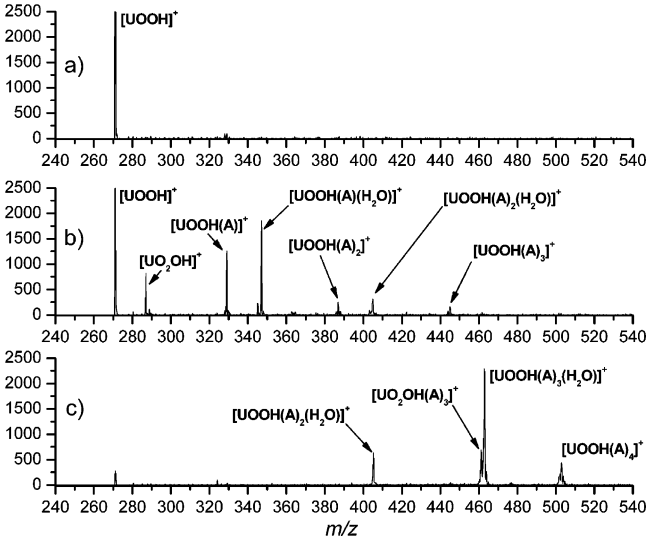

Figure 5. [UOOH]$^+$ formed and isolated in the vacuum atmosphere of the ion trap secondary ion mass spectrometer. Water and dioxygen were present at background concentrations ($\sim 5 \times 10^{-7}$ Torr), and acetone was added to a pressure of $\sim 1 \times 10^{-6}$ Torr. [UOOH]$^+$ reacted for (a) 0. (b) 0.06, and (c) 1 s.

means for forming the U(IV) species using electrospray. The [UOOH]$^+$ is an intriguing cation because uranium is in the IV oxidation state, with two electrons in the valence orbitals; thus, if occupation of these orbitals is solely responsible for reactivity with dioxygen, then there is a possibility that O_2 addition might also be observed in complexes of this ion.

The reactivity pattern for [UOOH]$^+$ (Figure 5) bore many similarities to that of $[UO_2]^+$, but with the following exceptions: (a) the [UOOH]$^+$ complexes did not add dioxygen, (b) complexes containing multiple H_2O ligands were not formed in abundance, and (c) a complex containing acetone and a H_2O ligand was the dominant product at the longest time scales accessible (the terminal addition product was primarily $[UOOH(A)_3(H_2O)]^+$, with lower abundance ions corresponding to $[UOOH(A)_4]^+$, $[UOOH(A)_2(H_2O)]^+$, and $[UO_2OH(A)_3]^+$ (Figure 5c)).

A careful examination of the temporal reaction profile showed initial production of the monoacetone complex $[UOOH(A)]^+$, $[UOOH(H_2O)]^+$ at lower abundance, and a minor amount of oxidation (vide infra). Once formed, $[UOOH(A)]^+$ displayed a dramatic preference for addition of H_2O (reaction 9, Scheme 6), this being preferred by a factor of 10 over addition of a second acetone ligand (reaction 2, and see reaction efficiencies in Tables 3 and S7). Conversely, the H_2O adduct preferred to add acetone (reaction 5, Scheme 6), and there was no tendency to add a second H_2O. Both reactions 5 and 9 produce the mixed-ligand adduct $[UOOH(A)(H_2O)]^+$, which is the most abundant ion after about 0.1 s of reaction time. The very fast appearance of this ion and the relatively large RMS value (Table S9) for the temporal profile of the $[UOOH(H_2O)]^+$ suggest that there may be a third contributor to $[UOOH(A)(H_2O)]^+$. It is speculated that some fraction of the diacetone adduct $[UOOH(A)_2]^+$ may be converted to $[UOOH(A)(H_2O)]^+$ by hyperthermal collisions with H_2O, and in fact collision-induced substitution reactions have been evidenced by the products of CID of uranyl complexes.[31]

Both $[UOOH(A)(H_2O)]^+$ and $[UOOH(A)_2]^+$ continue to add an additional ligand, as depicted in the kinetic profile (Figure 6) and by reactions 3, 6, and 10 (Scheme 6) and by reaction 12 (Scheme 6S). An important observation is that, despite the rapid addition of the first H_2O ligand, additions of subsequent H_2O ligands are somewhat disfavored (reaction 10 is particularly inefficient), presumably because the presence of two valence electrons in the U(VI) system together with two donor ligands generates enough repulsive character at the U center that approach of a weak donor is discouraged. A second surprising observation is that, at the longest time frames investigated (to 3 s), a complex containing one H_2O ligand $[UOOH(A)_3(H_2O)]^+$ was still most abundant and did not appear to be converting to the all-acetone complex $[UOOH(A)_4]^+$. The rate constants for elimination of acetone and H_2O from $[UOOH(A)_3(H_2O)]^+$ are slow (Table S8), which suggests that this ion is relatively stable. However, it is not expected to be as stable as the all-acetone

Table 3. Forward Rate Constants and Efficiencies Modeled for the Reactions of [UOOH]$^+$ in a Mixed Acetone, Water, and Dioxygen Atmosphere[a]

forward reaction	rate constant, $^{IV}k_n$	mean $^{IV}k_n$ value	% efficiency (relative to k_{ADO})
$[UOOH]^+ + A \rightarrow [UOOH(A)]^+$	$^{IV}k_1$	5×10^{-10}	20
$[UOOH(A)]^+ + A \rightarrow [UOOH(A)_2]^+$	$^{IV}k_2$	2×10^{-10}	10
$[UOOH(A)_2]^+ + A \rightarrow [UOOH(A)_3]^+$	$^{IV}k_3$	6×10^{-10}	30
$[UOOH(A)_3]^+ + A \rightarrow [UOOH(A)_4]^+$	$^{IV}k_4$	2×10^{-10}	10
$[UOOH(H_2O)]^+ + A \rightarrow [UOOH(A)(H_2O)]^+$	$^{IV}k_5$	2×10^{-09}	100
$[UOOH(A)(H_2O)]^+ + A \rightarrow [UOOH(A)_2(H_2O)]^+$	$^{IV}k_6$	3×10^{-10}	10
$[UOOH(A)_2(H_2O)]^+ + A \rightarrow [UOOH(A)_3(H_2O)]^+$	$^{IV}k_7$	1×10^{-10}	5
$[UOOH]^+ + H_2O \rightarrow [UOOH(H_2O)]^+$	$^{IV}k_8$	1×10^{-11}	30
$[UOOH(A)]^+ + H_2O \rightarrow [UOOH(A)(H_2O)]^+$	$^{IV}k_9$	2×10^{-09}	100
$[UOOH(A)_2]^+ + H_2O \rightarrow [UOOH(A)_2(H_2O)]^+$	$^{IV}k_{10}$	3×10^{-11}	1
$[UOOH(A)_3]^+ + H_2O \rightarrow [UOOH(A)_3(H_2O)]^+$	$^{IV}k_{11}$	3×10^{-10}	10

[a] The full set of rate constants for the $[UOOH]^+$ experiments are found in Tables S7 and S8 in the Supporting Information.

Scheme 6. Reaction Pathways for the Addition of Acetone and/or H_2O to $[UOOH]^+$[a]

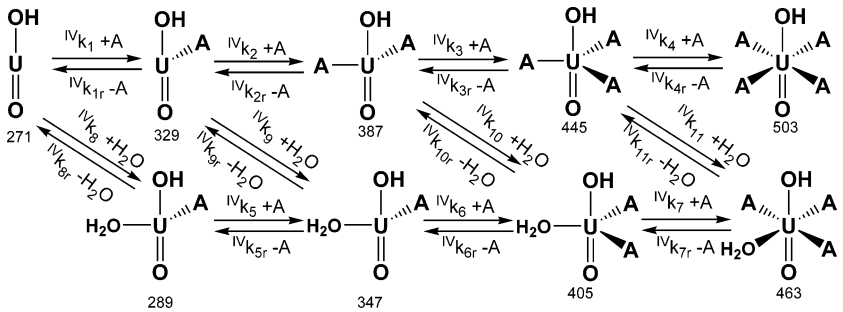

[a] The full scheme, including low-abundance ions, is found in the Supporting Information, Scheme 6S.

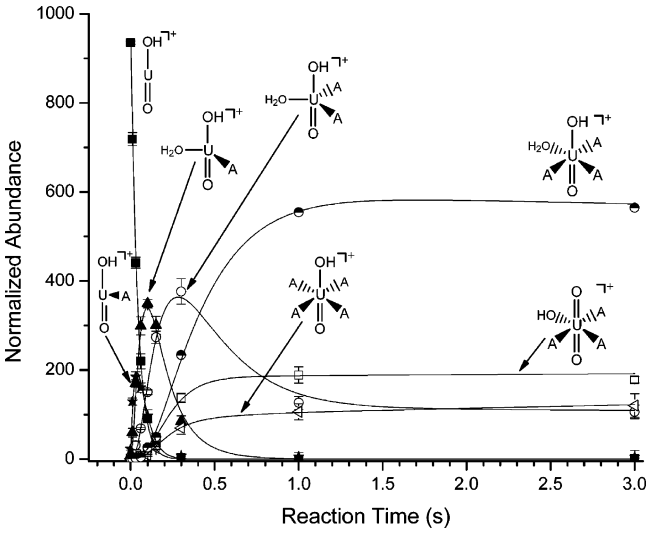

Figure 6. Kinetic profile for the major product ions produced from $[UOOH]^+$ in an atmosphere containing acetone, H_2O, and dioxygen. Data points represent the average of three runs. Lines represent the plot of the kinetic model for each of the ions. Low-abundance ion profiles are depicted in Figure S3 (Supporting Information).

system, suggesting that, at very long ion lifetimes, the all-acetone complex should be formed from the complex containing a single H_2O.

The U(IV) species did not add molecular O_2 at any point during the ligand addition reactions, but it did undergo irreversible oxidation with O_2 to form $[UO_2OH]^+$, with an efficiency ($^{IV}k_{11}$) that was in reasonable agreement with a previous measurement made using IT-SIMS.[30] The hydroxyuranyl cation proceeded to add acetone as shown in Schemes 1 and S3, with reactions occurring in parallel with the addition reactions of $[UOOH]^+$. An additional possibility for the appearance of the product $[UO_2OH(A)_n]^+$ cations is oxidation of acetone-ligated $[UOOH]^+$ precursors, as described by reactions 13−16 in Scheme 6S. Additional electron density from the strongly donating acetone ligands may actually make these reactions more efficient. Modeling of the kinetic profiles of these ions did not support this hypothesis but did suggest that, while $[UOOH(A)_n]^+$ oxidation was highly efficient for $n = 0$ and 2, complexes with one and three acetone ligands were largely unreactive. This result suggests that, as in the case of the dioxo U(V) complexes, the reactions of dioxo U(IV) complexes with dioxygen are very sensitive to alterations in the ligand field.

Conclusions

The addition of O_2 to ligated $[UO_2]^+$ complexes is reminiscent of additions to transition metal complexes,[19,20,22−24,64,65] where the availability of an unpaired electron and a higher oxidation state fosters formation of metal−superoxide complexes. The fact that prior equatorial ligation is required points toward specific involvement of the unoccupied or partially occupied valence orbitals of the uranyl system, which are two δ_u and two ϕ_u orbitals of 5f parentage[66,67] whose relative energy levels in ligated complexes are not known. Theoretical considerations would suggest that addition of the first two σ-donor ligands would involve the two 5f ϕ_u orbitals via an electrostatic interaction.[67] The resulting localization of the unpaired electron in a δ_u orbital may enable efficient overlap with the π^* orbital of dioxygen,[19,22,68] enabling formation of a weak covalent bond. Evidence for electron transfer from the metal center to an acceptor ligand has been observed for U(III) complexes in situations where π-back-bonding is possible,[69−73] but it has not been previously observed for U(V) complexes. Transfer of one electron from the U(V) center to O_2 would result in an η^1 superoxo complex, in which O_2 is attached end-on to the metal. In transition metal and actinide chemistry, dioxygen binding resulting in η^2-bound peroxy complexes is also common, but this requires two unpaired electrons, which are not present in the ligated $[UO_2]^+$ molecule. The role of the two donor ligands may be two-fold, i.e., localizing the unpaired electron in an orbital conducive to electron transfer to the π^* orbitals of O_2, as mentioned above, and increasing the overall basicity of the metal center. This explanation for the reactivity of ligated $[UO_2]^+$ thus bears some similarity to that offered by Mehdoui et al. for U(III) complexes, where stronger σ-donating ligands fostered stronger π-back-bonding with π-acceptor ligands.[74,75]

The candidate superoxo and peroxo structures would benefit from study using computational approaches, and in fact preliminary density functional theory calculations in our laboratories have generated not only an η^1 superoxo structure but also an η^2 side-bound peroxo structure. The variable results highlight the fact that DFT calculations of actinide complexes are not simple on account of relativistic effects and spin−orbit coupling,[76−78] and the present experimental measurements are in need of a determined computational investigation to provide a better understanding of the electronic configuration and reactivity of ligated forms of the $[UO_2]^+$ molecule and the structures of complexes resulting from their reactions.

Acknowledgment. The INL authors acknowledge support by the U.S. Department of Energy, Environmental Systems Research Program, under contract DE-AC07-05ID14517. M.J.V. and W.C. acknowledge support from the National Science Foundation (CAREER-0239800), the Kansas Technology Enterprise Corporation/Kansas NSF EPSCoR program, and a subcontract from the U.S. Department of Energy through the INL Institute. Funds for the purchase of the LCQ-Deca instrument were provided by the Kansas NSF EPSCoR program and the Wichita State University College of Liberal Arts and Sciences. The support of J. Oomens, N. Polfer, D. T. Moore,

(64) Wallace, W. T.; Wyrwas, R. B.; Whetten, R. L.; Mitric, R.; Bonacic-Koutecky, V. *J. Am. Chem. Soc.* **2003**, *125*, 8408−8414.
(65) Yoon, B.; Häkkinen, H.; Landman, U. *J. Phys. Chem. A* **2003**, *107*, 4066−4071.
(66) DeKock, R. I.; Baerends, E. J.; Boerrigter, P. M.; Snijders, J. G. *Chem. Phys. Lett.* **1984**, *105*, 308−316.
(67) Pepper, M.; Bursten, B. E. *Chem. Rev.* **1991**, *91*, 719−741.
(68) Cramer, C. J.; Tolman, W. B.; Theopold, K. H.; Rheingold, A. L. *Proc. Natl. Acad. Sci. U.S.A.* **2003**, *100*, 3635−3640.
(69) Bursten, B. E.; Strittmatter, R. J. *J. Am. Chem. Soc.* **1987**, *109*, 6606−6608.
(70) Bursten, B. E.; Rhodes, L. F.; Strittmatter, R. J. *J. Am. Chem. Soc.* **1989**, *111*, 2758−2766.
(71) Brennan, J. G.; Stults, S. D.; Andersen, R. A.; Zalkin, A. *Organometallics* **1988**, *7*, 1329−1334.
(72) Mazzanti, M.; Wietzke, R.; Pecaut, J.; Latour, J.-M.; Maldivi, P.; Remy, M. *Inorg. Chem.* **2002**, *41*, 2389−2399.
(73) Kaltsoyannis, N.; Scott, P. *Chem. Commun.* **1998**, 1665−1666.
(74) Mehdoui, T.; Berthet, J. C.; Thuery, P.; Ephritikhine, M. *Dalton Trans.* **2004**, 579−590.
(75) Mehdoui, T.; Berthet, J. C.; Thuery, P.; Ephritikhine, M. *Dalton Trans.* **2005**, 1263−1272.
(76) de Jong, W. A.; Visscher, L.; Nieuwpoort, W. C. *J. Mol. Struct.* **1999**, *458*, 41−52.
(77) Hay, P. J.; Martin, R. L.; Schreckenbach, G. *J. Phys. Chem. A* **2000**, *104*, 6259−6270.
(78) Schreckenbach, G.; Hay, P. J.; Martin, R. L. *J. Comput. Chem.* **1999**, *20*, 70−90.

and B. Redlich at the FOM Instituut voor Plasmafysica "Rijnhuizen", Nieuwegein, The Netherlands, in making the IRMPD measurement is gratefully acknowledged, as is the support of John Eyler (University of Florida) and the National Science Foundation (NSF grant CHE-9909502) for travel for G.S.G. and A.K.G.

Supporting Information Available: Several additional figures, tables, and schemes providing details on the results from mass spectrometric reactions are shown. This material is available free of charge via the Internet at http://pubs.acs.org.

JA0573209f